Investigating unconventional superconductivity in the 2D Hubbard-Kanamori model using Functional Renomarlization Group (FRG)

210003218

February-May 2025

Contents

1 Abstract

2 Introduction

3 Theoretical Background

3.1 Unconventional superconductivity

For many years after the discovery of superconductivity in 1911 [1] physicists were convinced that BCS-Eliashberg-electron-phonon theory [2] provided a complete explanation of the pairing mechanism in all superconducting materials. However, in 1986, the discovery of the first heavy-fermion superconductor [3] resulted in the emergence of a whole new class of materials: Unconventional Superconductors. These are condensates of cooper pairs formed by a **different** pairing mechanism than the electron-phonon coupling predicted by BCS theory. However, for some materials there is no wide agreement on what the mechanism otherwise is.

Most generally, the Hamiltonian for a superconducting state can be described as follows:

$$\hat{H} = \hat{H}^0 + \hat{H}^{cp} \tag{1}$$

where $\hat{H}^{cp}$ describes the pairing interation that leads to the formation of a Cooper pair and is given by:

$$\hat{H}^{cp} = \sum_{k,k'} \Gamma(k,k') c_{k,\uparrow}^\dagger c_{k',\downarrow}^\dagger c_{k',\uparrow} c_{-k,\downarrow} \tag{2}$$

In the case of unconventional superconductors, the form of the effective pairing interaction $\Gamma(k,k')$ has remained as an unanswered question for decades.

3.1.1 Spin-fluctuation mediated superconductivity

One emerging theory for some unconventional superconductors such Iron-based or heavy-fermion compounds is that underlying pairing mechanism is driven by spin fluctuations [4]. This section discusses how to model spin-fluctuation mediated superconductivity for the fluctuation-exchange approximation(FLEX) [5].

In such cases, the effective pairing interaction $\Gamma(k, k')$ is given by [1] [6] :

$$\Gamma(k, k') = \frac{3}{2}U^2\chi^S(k - k') - \frac{1}{2}U^2\chi^C(k - k') + U \tag{3}$$

where U is the on-site Coulumb repulsion and χ^S, χ^C are the interacting spin-susceptibilities in the Charge (C) and Spin(S) channel respectively. The later are given below.

$$\chi^S(q) = \frac{\chi^0(q)}{1 - U\chi^0(q)} \tag{4}$$

$$\chi^C(q) = \frac{\chi^0(q)}{1 + U\chi^0(q)} \tag{5}$$

These interacting spin susceptibilities are expressed in terms of the non-interacting dynamic spin susceptibility (χ^0_{ps}) which is stated below without formal proof [4].

$$\chi^0_{ps}(q, i\omega) = -\sum_k \int_0^\beta d\tau G^0_{ps}(k + q\tau)G^0_{sp}(k, -\tau)e^{i\omega\tau} \tag{6}$$

The calculations presented in this project are carried out in the spin-fluctuation framework. This theory has succesfully captured key features in phase diagrams of unconvential superconductors but also has its limitations. The most relevant example is that of the cuprate phase diagram. Spin-fluctuation theory is able to describe the superconducting dome and correct order parameter [7,8] and fails to describe the characteristic pseudo-gap [9].

3.2 Hubbard-Kanamori Model

3.2.1 Tight Binding Models

The Tight Binding Model is a central element of condensed matter physics (7). In this model, electrons are bound in orbitals (called sites) around the lattice ions. Due to the overlap between the quantum mechanical wavefunctions that describe these sites, electrons are allowed to 'hop' to neighbouring sites. The probability that this hopping process will occur is given by a tunnelling amplitude, which can be calculated using a hopping integral.

This work is carried out in the tight-binding model framework, where the magnitude of the tunnelling amplitudes are at first treated as free parameters. Here, we build from a simple 2D nearest-neighbour hoppping Hubbard model (Section. 3.2.2) and investigate the effect of

---

[1]Note that this form of pairing interaction assumes that the ratio between the fluctuation frequence w_f and the Fermi energy is small.

introducing and varying the strength of the next-nearest neighbour hopping amplitude (See Fig. 1). We extend these models further by considering the two-orbital per site case.

$$\hat{H}_{TB}(\underline{\mathrm{R}}) = \sum_{ij\sigma} t_{ij}(\hat{c}_{i\sigma}^{\dagger}\hat{c}_{j\sigma} + h.c) \tag{7}$$
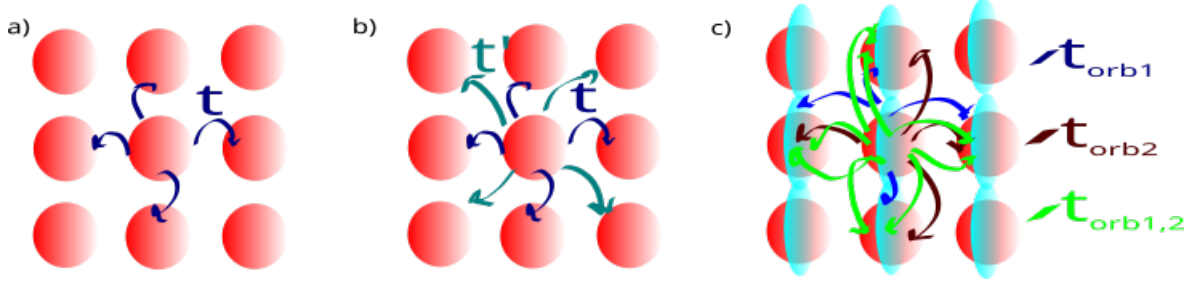
Figure 1: **Two-Dimensional Tight-Binding Models:** Three pannels showing the tight binding models for the 1NN, 1NNN and 1NN2 models discussed in Section 5.1, 5.2 and 5.3 respectively. Fig a) shows the Nearest-neighbour hopping case, where t depicts the hopping amplitude between the neighbouring sites. Fig b) shows the inclusion of the next-nearest neighbour hopping, the magnitude given by t'. Fig c) Shows the extension to the two-orbital case, depicting same orbital (t_{orb1}, t_{orb2}) and different orbital ($t_{orb1,2}$) nearest-neighbour hopping. Note that this is just a pictorial representation of the orbitals, and that it does not correspond to a particular choice of orbitals or their real space projection.

3.2.2 Hubbard Model

The tight binding model as defined above fails to account for any interactions between neighbouring electrons. This motivates the extension of this model to the Hubbard model (8), which includes the (onsite) Coulomb repulsion between electrons. Despite its simple form, this model can describe very rich physical phenomena. In particular, it becomes very interesting to study when U and t are of comparable order, since it highlights the competing phenomena that takes place in correlated systems. The 2D Hubbard model remains unsolved to date, but is able to predict all sorts of correlated phases: it describes metals, insulators, superconductors and other exotic phases (REFERENCE). This model has been widely studied since it resembles the structure of the cuprate high-temperature superconductors (REFERENCE).

$$\hat{H} = \sum_{ij\sigma} -t_{ij}(\hat{c}_{i\sigma}^{\dagger}\hat{c}_{j\sigma} + h.c) + U \sum_{i} \hat{n}_{i\uparrow}\hat{n}_{i\downarrow} \tag{8}$$

3.2.3 Hubbard-Kanamori Model

In the case of materials with a multi-band and/or multi-orbital nature, the Hubbard model is not sufficient to capture all of the physical phenomena. This motivates the extension of the Hubbard Model to the Hubbard-Kanamori model by including a Hund's coupling term.

$$H_{int} = U \sum_{is} n_{i,s\uparrow}n_{i,s\downarrow} + \frac{V}{2} \sum_{i,s,t \neq s} n_{is}n_{it} - \frac{J}{2} \sum_{i,s,t \neq s} \vec{S}_{is} \cdot \vec{S}_{it} + \frac{J'}{2} \sum_{i,s,t \neq s} \sum_{\sigma} c_{is\sigma}^{\dagger}c_{is\bar{\sigma}}^{\dagger}c_{it\bar{\sigma}}c_{it\sigma} \tag{9}$$

Here, U and V represent the electronic interactions in the same and different orbitals respectively. For generality, the intraorbital exchange J and the 'pair hopping' term J' following from Hund's rule coupling have been separated. Note that this Hamiltonian is relevant for the later section of this project, where the model is extended to a two-orbital, two-dimensional Hubbard Model.

3.3 Theoretical Background in FRG

Solving the Hubbard-Kanamori Hamiltonian is rather challenging, which is why we resort to numerical techniques such as FRG to do so. FRG falls into the category of many other weak-coupling techniques (such as Mean field-theory, pertubation theory...). In these theories, interactions between electrons are considered to be weak. This allows one to effectively model the electrons in the system as free particles and treat their interactions as a pertubation. In the non-interacting limit, the method is therefore exact. Beyond this limit, it is controlled by the ratio between the interaction strength and the bandwidth of the system.

In this section the theoretical framework in which FRG calculations are performed is outlined. The central element of FRG is a flow equation that describes the evolution of the effective action of the system with respect to a scalar/flow parameter Lambda Λ *(See section 3.3.1)*. The flow equation can be solved exactly for a limited number of systems (REFERENCE), so for most scenarios an approximation has to be made in order to reach a solution in a reasonable computational time. More details of how this approximation is performed and the limitations

it presents can be found in Section 3.3.2. For the systems explored in this project only two-particle interactions are considered and any higher order terms are neglected. This allows for the effective action of the system to be separated into three terms, which correspond to three physical channels: Superconductivity, Spin-Density and Charge-Density Waves. The calculation is then performed to determine the "winning channel" which will correspond to the respective physical phase that the model exhibits. This rather "hand-wavy" overview of FRG is represented in a flowchart in Fig.2. For a more rigorous explanation the reader is referred to the sections below.
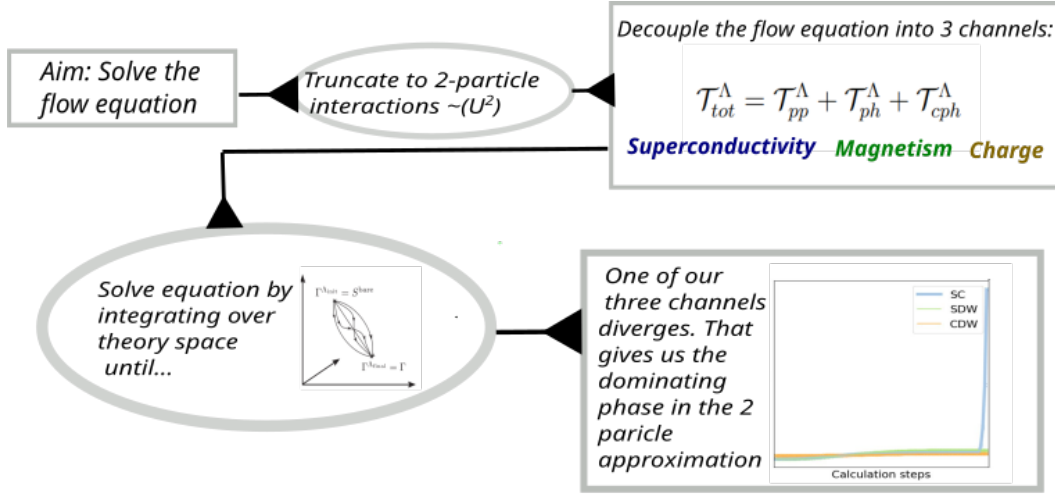

Figure 2: **FRG Flowchart:** Schematic diagram outlining the TU^{2}FRG calculation steps. Starting from the flow equation and applying the truncation scheme in order to decouple the action into three "physical" terms. The flow equation can then be solved by calculating each channel separatedly and taking the dominating phase to be the channel that diverges.

3.3.1 Flow equation

In this section the derivation of the flow equation is outlined. For such, it is assumed that the reader has grasped a strong understanding in Quantum Field theory and many-body physics. If interested in the finer details of the derivation, the reader is refferred to (REFERENCE).

The central elements of statitiscal physics are the partition function, the canonical potential and its Legendre transformations. These are such powerful physical quantities that one can derive all physical observables from them. For quantum many-body problems, one works instead with partition functional, defined as follows in Eq.10:

$$\mathcal{Z}[\bar{\eta}, \eta] = \int \mathcal{D}\bar{\psi}\mathcal{D}\psi e^{\mathcal{S}[\bar{\psi}, \psi]} e^{(\bar{\eta}, \psi) + (\eta, \bar{\psi})} \tag{10}$$

In the case of fermionic systems, the action in the exponent of Eq.10 takes the form shown below.

$$\mathcal{S}[\psi, \bar{\psi}] = -(\bar{\psi}, G_0^{-1}\psi) + V[\psi, \bar{\psi}] \tag{11}$$

Here, $V[\psi, \bar{\psi}]$ is an arbitrary many-body interaction and G_0 represents the propagator of the non-interacting system. This equation contains the shorthand notation (...), which represents the sum $\sum_x \bar{\psi}(x)(G_0^{-1}\psi)(x), (G_0^{-1}\psi)(x) = \sum_{x'} G_0^{-1}(x, x')\psi(x')$. In this sum, the Grassman field index x represents all the quantum numbers of the single-particle basis and imaginary time.

Note that in the limiting case where $V = 0$, the path integral in Eq.10 is exactly solveable. However, once electronic correlations are included, the picture becomes more complicated. The main idea behind FRG is to introduce a cut-off in the non interacting Green's function ($G_0 \rightarrow G_0^\lambda = f(\lambda)G_0$). This cutoff is then interpolated between the solveable intital state and the full path integral solution by susbsequently including electronic interactions. For a spin-independant system this would transform the bare propagator as shown in Equations (12) and (13).

$$G_0(k_0, \mathbf{k}) \rightarrow G_0^\lambda(k_0, \mathbf{k}) \tag{12}$$

$$\frac{1}{ik_0 - \xi_\mathbf{k}} \rightarrow \frac{\theta^\mathbf{k}}{ik_0 - \xi_\mathbf{k}} \tag{13}$$

where $\theta^\lambda(\mathbf{k})$ is defined, for example, as follows:

$$\theta^\lambda(\mathbf{k}) = \Theta(|\xi_\mathbf{k}| - \lambda) \tag{14}$$

With this cutoff scheme, the calculation then excludes points close to the Fermi Surface as shown in Figure (FIGURE).

In the following steps the derivation will proceed in the framework of the so-called "effective action" ($\mathcal{T}[\psi, \bar{\psi}]$). This is the Legendre transformation of the Greens function functional ($\mathcal{G}[\eta, \bar{\eta}]$), defined below in Equations (15, 16) and (17) respectively. *(For convinience and for reasons that are beyond the scope of this project it is more convinient to work with the effective action than it is to do so with the partition functional.)* [2]

$$\mathcal{G}[\eta, \bar{\eta}] = -ln(\mathcal{Z}[\eta, \bar{\eta}]) \tag{15}$$

$$\mathcal{G}[\eta, \bar{\eta}] = -ln \int \mathcal{D}\psi \mathcal{D}\bar{\psi} e^{-\mathcal{S}[\psi, \bar{\psi}]} e^{(\bar{\eta}, \psi) + (\bar{\psi}, \eta)} \tag{16}$$

$$\mathcal{T}[\psi, \bar{\psi}] = (\bar{\eta}, \psi) + (\bar{\psi}, \eta) + \mathcal{G}[\eta, \bar{\eta}] \tag{17}$$

The next step is to introduce a scalar flow parameter λ into the generating functionals defined above. This is done in the same manner as is outlined in the example shown in Equations (12, 13). But more generally, has to be performed such that the generators recover their orginal structure at $\lambda = 0$. After a series of algebraic manipulations, which are ommitted here but can

---

[2]If interested in why see REFERENCE

be found in (REFERENCE), one arrives at the exact functional flow equation for the effective action:

$$\frac{d}{d\Lambda}\mathcal{T}^{\Lambda}[\psi,\bar{\psi}] = (\bar{\psi}, \dot{Q}_0^{\Lambda}\psi) - \frac{1}{2}\text{tr}\big(\dot{Q}_0^{\Lambda}(\mathbf{\Gamma}^{(2)\Lambda}[\psi,\bar{\psi}])^{-1}\big). \tag{18}$$

Where $\Gamma^{(2)\lambda}[\psi,\bar{\psi}]$ and $\underline{Q}_0^{\Lambda}$ are given by equations (19) and (20) respectively.

$$\Gamma^{(2)\lambda}[\psi,\bar{\psi}] = \begin{bmatrix} \bar{\delta}\delta\Gamma[\psi,\bar{\psi}](x',x) & \bar{\delta}\bar{\delta}\Gamma[\psi,\bar{\psi}](x',x) \\ \delta\delta\Gamma[\psi,\bar{\psi}](x',x) & \delta\bar{\delta}\Gamma[\psi,\bar{\psi}](x',x) \end{bmatrix} \tag{19}$$

$$\underline{Q}_0^{\Lambda} = \begin{bmatrix} Q_0^{\Lambda} & 0 \\ 0 & -Q_0^{\Lambda t} \end{bmatrix} = diag(Q_0^{\Lambda}, -Q_0^{\Lambda t}), \tag{20}$$

This equation, as mentioned previously, is the central element of FRG and the sections below outline how to solve it.

3.3.2 Truncation scheme (TU^{2}FRG)

The flow equation derived above can be solved for a limited amount of systems (REFERENCE). However, in most cases, the memory demand for the FRG calculations is high. In order to tackle this issue, the truncated unity approximation (TU^{2}FRG) was introduced in 2020 (REFERENCE). The main idea behind this scheme is to find a new basis that, with a controlled loss of accuracy, can represent all of the required elements in a compressed way. It can be shown (REFERENCE), that such a basis can be constructed and is well defined in the case where the calculation is constrained to terms U^2 *(two-particle interactions)*. Partitions of unity [3] are then introduced into a specific part of the flow equation. This reduces an otherwise computationally expensive nested integral to a matrix product. Details of how this truncation is incorporated are ommitted but the reader is referred to Appendix. (REFERENCE appendix).

Whilst the truncated scheme presents advantages in computational efficiency, particularly for models with broken translational symmetry, it also has its limitations. TU^{2}FRG relies on short-range interactions, thus struggling to capture strongly correlated phases. This is particularly relevant for the study of the 2D Hubbard model. TU^{2}FRG will not be able to capture the characteristic Mott insulating phase of the Cuprate phase diagrams (REFERENCE), which limits how well the results presented in this project can be directly compared with existing literature. Nevertheless, it manages to successfully capture the competition between Magnetic and Superconducting instabilities, which is one of the main focus of the results presented here.

3.3.3 Decoupling of flow equation

After constraining ourselves to the case of two-particle interactions in the framework of translationally invariant systems, one can decouple the evolution of the two-particle coupling as a function of the flow parameter λ into three channels:

---

[3]A detailed explanation of what these are can be found in

$$V(k1, k2, k3) = V^{(0)}_{k_1, k_2, k_3} - \phi^P_{k_1+k_2, \frac{k_1-k_2}{2}, \frac{k_4-k_3}{2}} + \phi^C_{k_1-k_3, \frac{k_1+k_3}{2}, \frac{k_2+k_4}{2}} + \phi^D_{k_3-k_2, \frac{k_1+k_4}{2}, \frac{k_2+k_3}{2}} \tag{21}$$

Here, the three channels correspond to a particle-particle, crossed particle-hole and (three) direct particle-hole terms given explicitly below in terms of the respective effective actions. They represent all possible ways in which the two particle interactions can occur in the correlated system. The particle-particle (P), cross-particle-hole (C) and direct-particle-hole (D) channels correspond to the Superconducting, Charge and Magnetic phases respectively.

$$\dot{\phi}^P_{k_1+k_2, \frac{k_1-k_2}{2}, \frac{k_4-k_3}{2}} = -\mathcal{T}_{pp}(k1, k2, k3) \tag{22}$$

$$\dot{\phi}^C_{k_1-k_3, \frac{k_1+k_3}{2}, \frac{k_2+k_4}{2}} = -\mathcal{T}_{cr-ph}(k1, k2, k3) \tag{23}$$

$$\dot{\phi}^D_{k_3-k_2, \frac{k_1+k_4}{2}, \frac{k_2+k_3}{2}} = -\mathcal{T}_{d-ph}(k1, k2, k3) \tag{24}$$

This effectively allows one to treat the effective action as a separable object:

$$\mathcal{T}[\psi, \bar{\psi}] = \mathcal{T}_{pp}[\psi, \bar{\psi}] + \mathcal{T}_{ph}[\psi, \bar{\psi}] + \mathcal{T}_{cph}[\psi, \bar{\psi}] \tag{25}$$

3.3.4   Instability calculation

The procedure from the decoupled effective action and flow equation is outlined here. For more details the reader is refferred to (REFERENCES). A FRG calculation will return the self-energy and two-particle vertex [4]. These quantities are not directly experimentally accessible, so a series of post processing steps have to be carried out. The first step is to find out which of the three channels diverge. This gives the diverging susceptibility. Mean-Field analysis is then carried out at the critical scale in order to obtain the ordering symmetry and a linearised gap equation. The later allows one to calculate the Superconducting gap and order parameter.

4   Computational Methods

This section outlines how the concepts presented above link together and are implemented for the purpose of this project. The general aim is to solve the Hubbard-(Kanamori) model for the 2D Hubbard model. This is achieved computationally, using the Diverge package. This package implements the TU^{2}FRG formalism discussed in the section above. All of the calculations are carried out under the assumption that the superconductivity is spin-fluctuation mediated. This section outlines the methods followed to calculate the required Tight-Binding Models for each of the systems, the utilisation of Diverge and some of the post-processing techniques used.

---

[4]This is the footnote text.

4.1 Tight-Binding Models

This project discusses three models: the 1NN, 1NNN and 1NN2 model (*See Fig.1*). For the first two, the hopping parameters in the tight-binding model are treated as free parameters. For the later, the hopping parameters are determined using the method described below.

Constrained to the case of a single layer, the 1NN model is extended to a multi-orbital system by including two-orbitals per site and investigating the effect of the interorbital hopping. To allow for comparison with exisiing literature (REFERENCE), a $d_{x^2-y^2}$ and $d_{3z^2-r^2}$ orbital are including. Their respective hopping parameters are calculated using the table of interatomic matrix elements calculated by J.C. Slater and G.F. Koster [10]. In this calculation, the values of the σ, π, δ bond strength are approximated to $\approx 1, 0.5, 0.05 eV$ respectively in order to capture their relative values (REFERENCE). A table summarising estimated parameters for the models discussed in Section 5.3 is shown below.

Model	$t^{[1,0,0]}_{3z^2-r^2}$	$t^{[0,1,0]}_{3z^2-r^2}$	$t_{x^2-y^2}$	$t^{[1,0,0]}_{x^2-y^2-3z^2-r^2}$	$t^{[0,1,0]}_{x^2-y^2-3z^2-r^2}$
	-0.781	-0.719	-0.375	-0.402	-0.310
1NN2MN	on	on	on	off	off
1NN2MY	on	on	on	on	on

Table 1: **Nearest neighbour hopping parameters for 2D two-orbital Hubbard models.** First row shows the calculated hopping parameters. Other rows show which hopping parameters were included in each of the two models.

4.2 Diverge

4.3 Convergence of Calculation

4.3.1 Form factor convergence

4.3.2 Number of k points convergence

4.4 Calculation of Susceptibilities

4.4.1 Nesting vectors

4.4.2 Superconducting order parameters

5 Results and discussion

5.1 1NN Model

We define the 1NN model as the 2D Hubbard model with a single orbital per site, allowing hopping between nearest-neighbour sites *(a diagramatic representation can be found in Fig.1.a)*. As outlined in Section 3.2.2, solving this model near half-filling becomes a hard endeavour.

This section explores the solution to the 1NN Model Hamiltonian using two-particle-interaction-truncated FRG. Here, a phase diagram in terms of the On-site Coulomb repulsion U and chemical potential μ is presented and discussed in detail. The calculations were carried out using a 20x5 n_kxn_{kf} grid and a form factor of 4Å, with a nearest-neighbour hopping parameter of 1eV. The choice of convergence parameters was determined by the methods discussed in Section 4.3. Results are presented for Coulomb repulsion values ranging from 1-20 eV and chemical potential values spanning the entire energetic bandwith of the model (from -4eV to 4eV). Whilst there exists previous work on the 2D Hubbard Model using FRG (REFERENCE), most of it focuses on small areas of the phase diagram and none of it explores the effect of varying the onsite Coulomb repulsion. Therefore, the work presented here covers a much wider range of parameters than what has previously been explored.

In real materials, the chemical potential is an easily tuneable parameter due to its strong connection to the electronic doping of the system. However, controlling the magnitude of the Coulumb repulsion between electrons is not that straightforward. Moreover, some of the interesting features discussed in this report lie outside of the physical regime. (ie- in our FRG calculation a weak-coupling limit was assumed and therefore any Coulomb repulsion values above the magnitude of the bandwidth of the material (8eV) can be considered to be unphysical in this limit.) Therefore, the analysis performed in this project does not neccesarily provide a route to enhance the superconductivity in real materials that resemble the models investigated. Instead, the main aim is to understand how varying these parameters affects the correlated phases observed in the model. It is also important to note, as discussed in Section 3.3.2, that any analysis on the transition temperature of the superconducting regions must be treated qualitatively and that this work does not claim to have found Superconducting regions at temperatures of the order of thousands of Kelvin in any of the models discussed.

The complete phase diagram for the values discussed above is shown in Fig.3. This particle-hole symmetric phase diagram shows a magnetic dome sandwiched between two superconducting regions. Moreover, narrow magnetic stirpes appear for even integer chemical potential values.
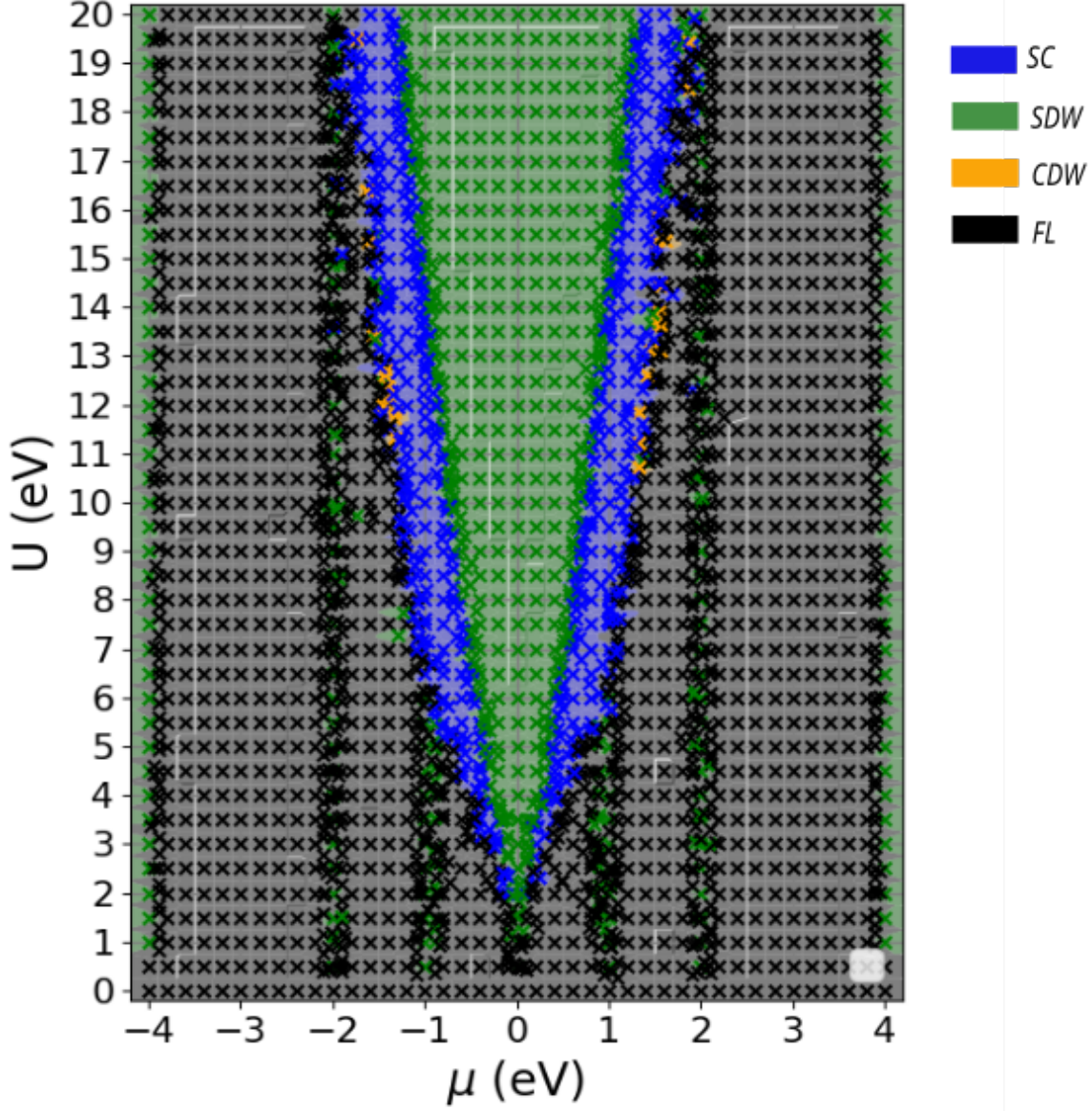
Paragraph comparing results to the Cuprates!

Figure 3: **Phase diagram for the 1NN model**: (t = 1eV, nkxnkf = 20x5, ff = 4Å) as a function of On-site Coulumb Repulsion U and chemical potential μ. Figure shows the four phases observed in the 1NN model: SC (Superconductivity), SDW (Spin-Density Wave), CDW(Charge Density Wave) and FL (Fermu-Liquid). Calculated points in the phase diagram are showed by the 'x' markers and a lighter-couloured background is used to depict interpolated regions between these points.
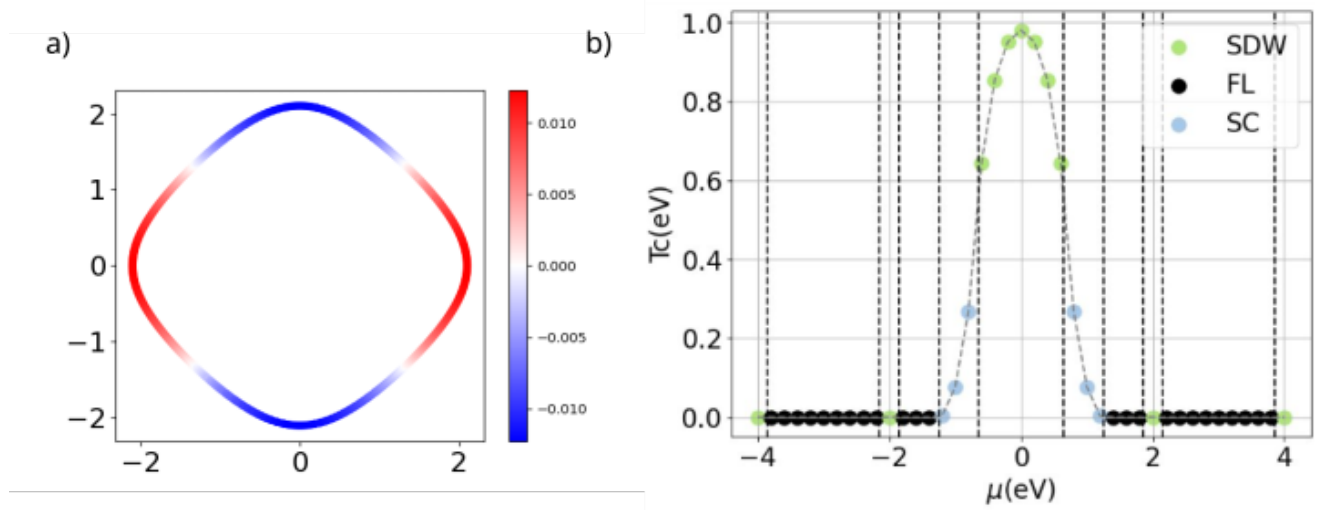
5.1.1 Superconductivity in the 1NN Model

Figure 4: **Superconductivity in the 1NN model**: Fig a) Superconducting order parameter projected on Fermi Surface at $\mu = 1.00$ eV, for U =10.00eV. The order parameter is antisymmetric about a 90 degree rotation and hence it exhibits d-wave symmetry. Fig b) Transition temperature (Tc) as a function of chemical potential (μ) for U =10.00eV. Tc is enhanced closest to the magnetic instability.

5.1.2 Magnetic stripes in the 1NN Model

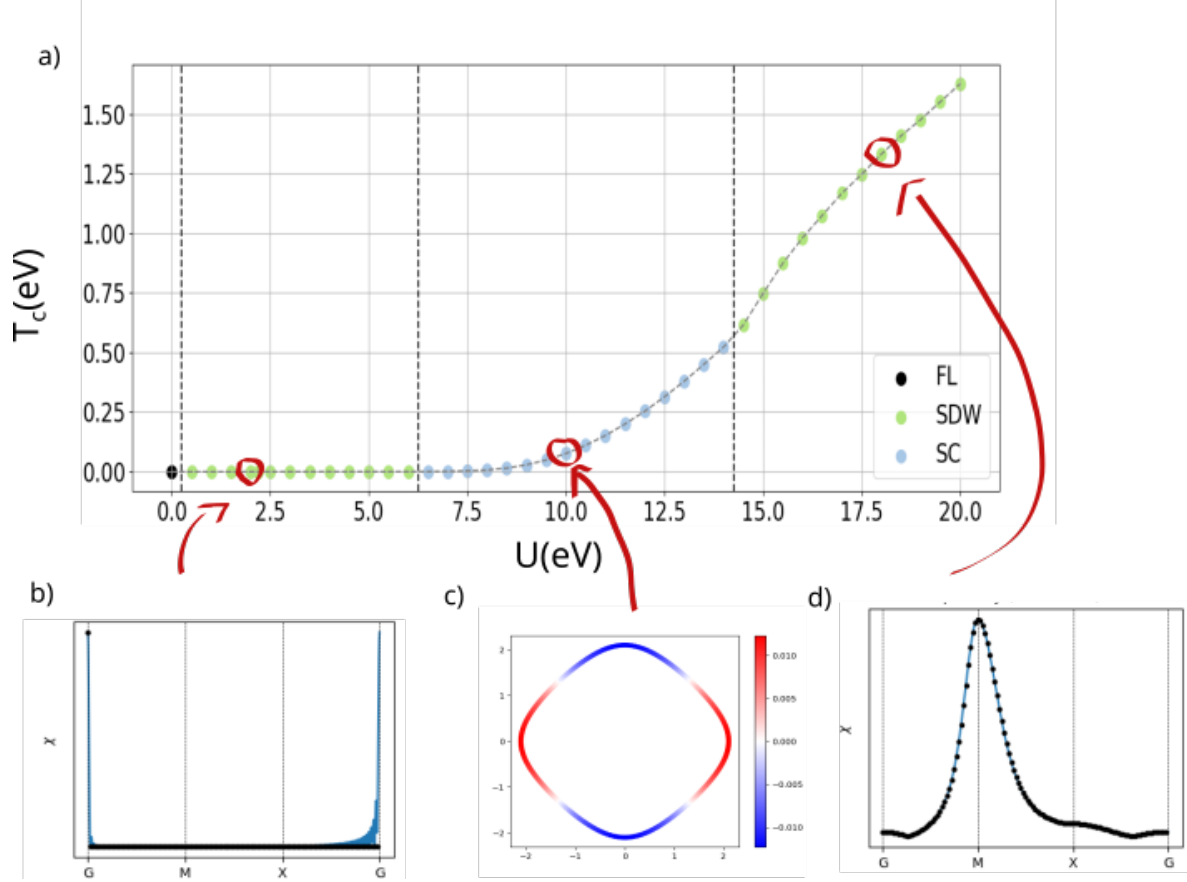## 5.2 Effect of next-nearest neighbour hopping (1NNN model)

Figure 5: **Magentic stripe in the 1NN model for doping at $\frac{1}{8}$ of the bandwith**: Fig a) Transition temperature as a function of Coulumb repulsion (U) along the Magnetic stripe at μ =1eV. Fig b) Magnetic susceptibility along high symmetry path for U =2.00 eV. Fig c) Plot of the Superconducting order parameter projected on top of the Fermi-surface of the 1NN model for U = 10.00eV and μ =1.00eV. Fig d) Magenetic susceptibility along high symmetry path for U= 18.00eV. Plots showing the susceptibility as a function of q for both magnetic regions. The Ferromagnetic SDW is supressed by a superconducting phase at U≈ 6.00eV. At larger values of U, the SDW phase is recovered but with an Anti-Ferromagnetic ordering instead.
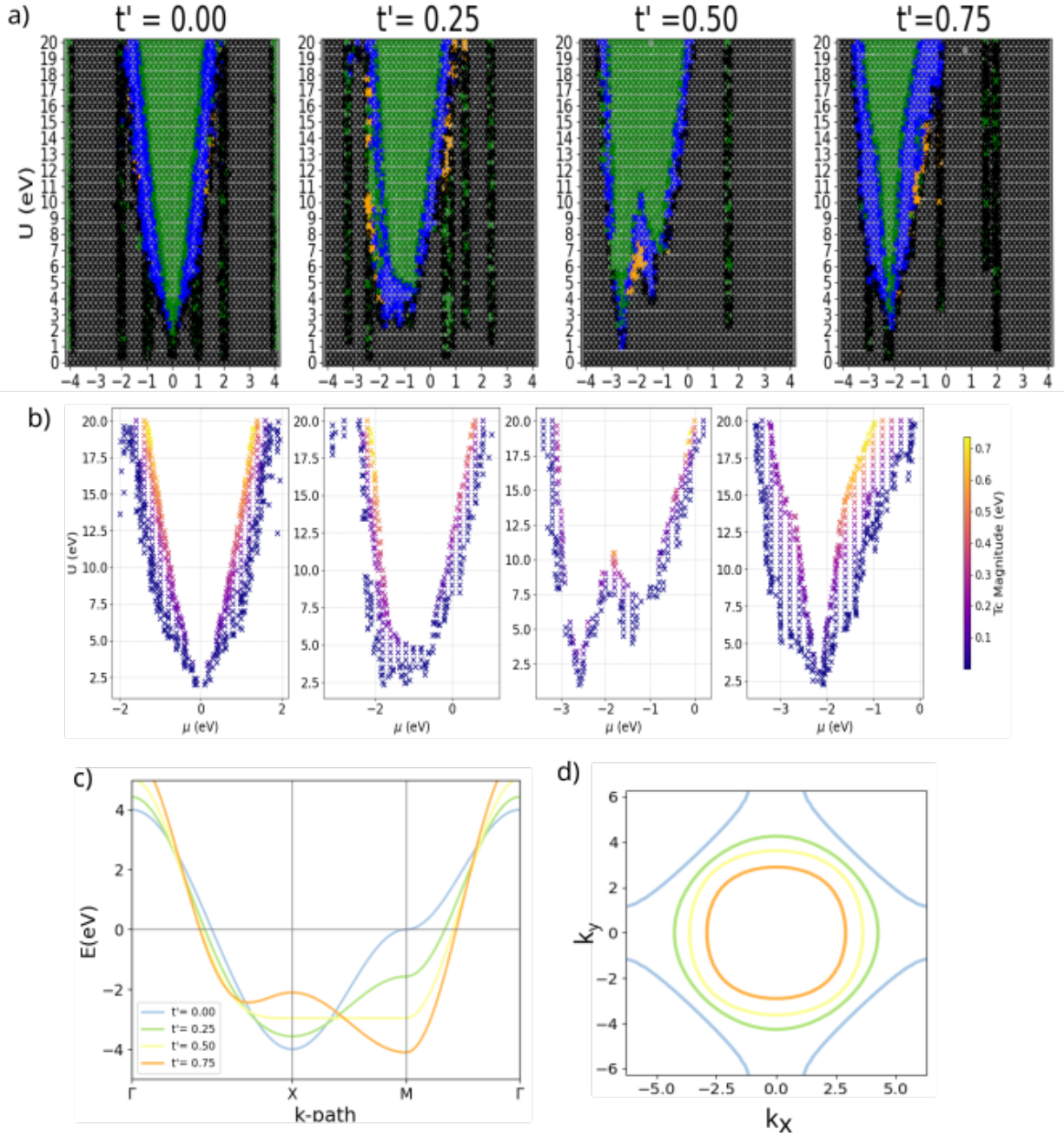
Figure 6: **1NNN model:** a) Phase diagram for the 1NNN model as a function of Coulumb repulsion U and chemical potential μ (t =1eV, nkxnkf = 20x5, ff = 4Å) for t'=0.00, 0.25, 0.50, 0.75 eV. b) Transition temperature for the superconducting region. c) Single plot of the band structure along high-symmetry path for corresponding values of t'. d) Single plot of the Fermi surface for all values of t' considered.

5.2.1 Superconductivity in the 1NNN Model

Important to note that results shown in Fig 7 are the plots for the case of U = 9.00eV and although this value is unphysical since we constrain ourselves to the weak-coupling approximation in which we assume that U is of the orders of magnitude of the bandwidth of the material.
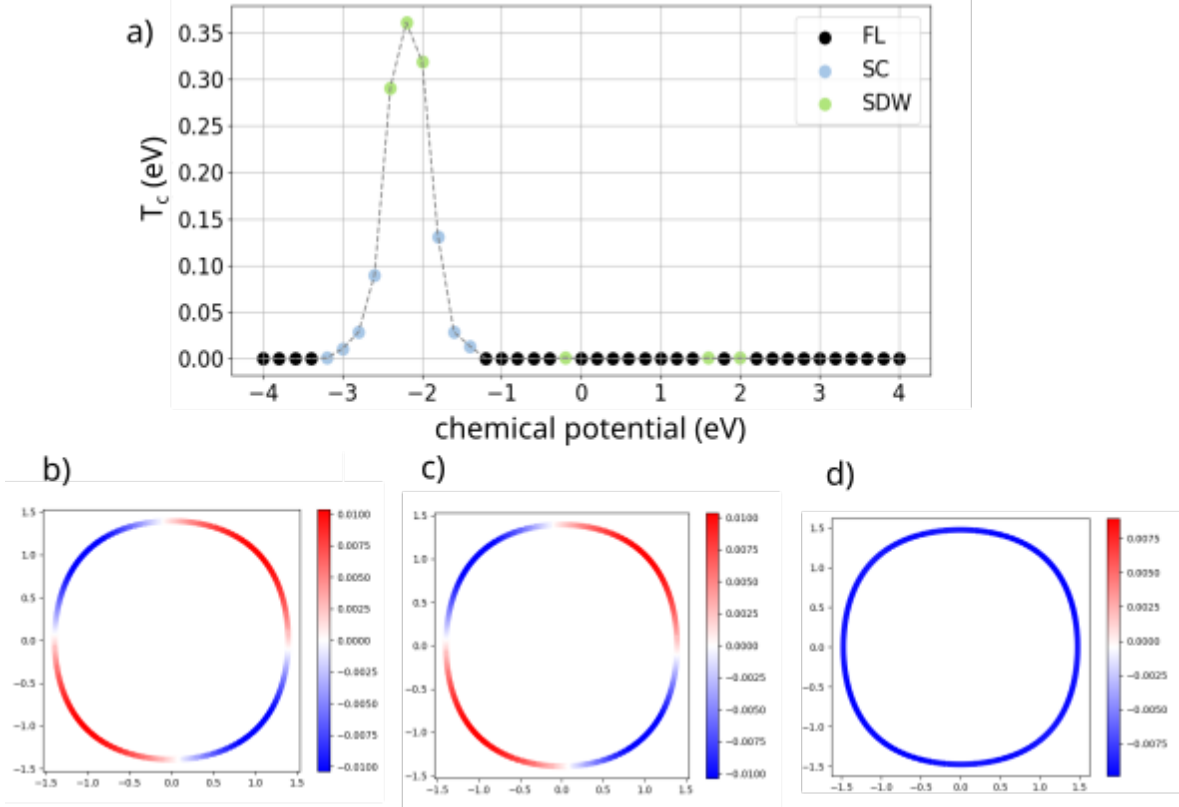

Figure 7: **Change in the superconducting order parameter in the t' =0.75eV 1NNN model**: Fig a) Critical temperature as a function of chemical potential μ for u = 9.00eV. The lower panel shows the magnitude of the superconducting order parameter plotted on top of the fermi surface for U= 9.00eV and μ = -2.6eV, -1.8eV and -1.4eV. These are shown in Figs b) c) and d) respectively.

5.2.2 Magnetic stripes in the 1NNN model

5.2.3 Continous variation of next-nearest neighbour hopping

5.3 Effect of bi-orbital system (1NN2 model)

5.3.1 Superconductivity in the 1NN2 model

5.3.2 Effect of orbital hybridisation in the 1NN2 model

6 Conclusion and Outlook

t'(eV)	μ (eV)	Competing with other phase?	Nesting vector	Magnetic ordering
0.00	1.00	Yes (SC)	(0,0)-(π, π)	Changing from FM-AFM
0.00	2.00	No	(0,0)-(0, π)	Changing from FM to Commensurate
0.25	2.40	No	(0,0)	FM
0.25	1.40	Yes (CDW)	(0,0)	FM
0.25	-2.00	No	(0,0)-(π, π)	FM - AFM
0.25	0.60	No	(0,0)	FM

Table 2: **Survey of stripes in the 1NNN model.** Table summarising the location and magnetic ordering of the Stripes in the 1NNN model .

References

[1] H Kamerlingh Onnes. The superconductivity of mercury. *Comm. Phys. Lab. Univ. Leiden*, 122:124, 1911.

[2] J Robert Schrieffer. *Theory of superconductivity*. CRC press, 2018.

[3] J George Bednorz and K Alex Müller. Possible high t c superconductivity in the ba- la- cu- o system. *Zeitschrift für Physik B Condensed Matter*, 64(2):189–193, 1986.

[4] Toru Moriya and Kazuo Ueda. Spin fluctuations and high temperature superconductivity. *Advances in Physics*, 49(5):555–606, 2000.

[5] Gökhan Esirgen and NE Bickers. Fluctuation-exchange theory for general lattice hamiltonians. *Physical Review B*, 55(4):2122, 1997.

[6] AB Migdal. Interaction between electrons and lattice vibrations in a normal metal. *Sov. Phys. JETP*, 7(6):996–1001, 1958.

[7] Toru Moriya. Developments of the theory of spin fluctuations and spin fluctuation-induced superconductivity. *Proceedings of the Japan Academy, Series B*, 82(1):1–16, 2006.

[8] Douglas J Scalapino. The case for dx2- y2 pairing in the cuprate superconductors. *Physics Reports*, 250(6):329–365, 1995.

[9] Tom Timusk and Bryan Statt. The pseudogap in high-temperature superconductors: an experimental survey. *Reports on Progress in Physics*, 62(1):61, 1999.

[10] John C Slater and George F Koster. Simplified lcao method for the periodic potential problem. *Physical review*, 94(6):1498, 1954.